Effects of GaAs substrate misorientation on strain relaxation in $In_xGa_{1-x}As$ films and multilayers

R. S. Goldman[a)]
Department of Materials Science and Engineering, The University of Michigan, Ann Arbor, Michigan 48109-2136

K. L. Kavanagh and H. H. Wieder
Department of Electrical and Computer Engineering, University of California, San Diego, La Jolla, California 92093-0407

S. N. Ehrlich
School of Materials Engineering, Purdue University, West Lafayette, Indiana 47907

R. M. Feenstra
Department of Physics, Carnegie Mellon University, Pittsburgh, Pennsylvania 15213

(Received 21 November 1997; accepted for publication 5 February 1998)

We have investigated the effects of GaAs substrate misorientation on strain relaxation in $In_xGa_{1-x}As$ films and multilayers. Our calculations of shear stresses due to misfit strain, resolved on the glide plane in the glide direction, reveal that the α and β 60° slip systems are influenced in a nearly identical fashion, for all substrate misorientation directions. Thus, classical models for nucleation and glide of 60° dislocations predict that a substrate misorientation will not influence the degree of $\langle 110 \rangle$ asymmetry in strain relaxation in lattice-mismatched zincblende semiconductor films. Contrary to these predictions, our experimental results reveal asymmetries in strain relaxation (for partially relaxed single layers) which favor those dislocations aligned with the offcut axis. These asymmetries depend on the substrate misorientation and growth temperature, and are not easily explained by differences in the intrinsic core properties of α and β dislocations. Furthermore, in fully relaxed multilayers (grown at lower temperatures), and single layers (grown at higher temperatures), epilayer tilt which increases the $(111)B$ substrate miscut is observed. In the multilayers, this behavior is found to be correlated with the presence of micron-scale surface facets. We consider possible explanations for these results, including nucleation of partial dislocations, interaction of gliding threading dislocations, and strain relaxation predominated by forward and backward gliding α threading dislocation segments. Together, these results support the conclusion that local surface or interface step morphologies are more important than bulk stress effects in determining misfit dislocation formation in the InGaAs/GaAs system. © *1998 American Institute of Physics.* [S0021-8979(98)03310-6]

I. INTRODUCTION

In lattice-mismatched III-V compounds, with mismatch less than about 1.5%, strain relaxation occurs primarily by the formation of 60° $a/2\ \langle 110 \rangle\ \{111\}$ misfit dislocations. These glide to the interface on {111} planes, where their Burger's vector, $a/2\ \langle 110 \rangle$, makes a 60° angle with the $\langle 110 \rangle$ line direction. The dislocations have edge and screw type interfacial components, and a tilt component perpendicular to the interface. If all possible dislocations are generated with equal probability, the screw and tilt components cancel out, leaving a net misfit component which relaxes the strain equally in both $\langle 110 \rangle$ directions. However, in zincblende crystals, two types of 60° dislocations are possible, α and β, which have $[\bar{1}10]$ and $[110]$ line directions at compressively stressed interfaces, presumably with Ga- and As-based cores. The different core structures of α and β dislocations are expected to lead to significant differences in activation energies for dislocation nucleation and glide. In undoped and n-type GaAs, it has been found experimentally that α dislocations have a higher glide velocity than β dislocations.[1,2] Thus, it is not surprising that α dislocations are often reported to form first during strain relaxation at n-type InGaAs/GaAs interfaces.[3] However, several recent reports of n-type growth of InGaAs on misoriented GaAs substrates have indicated the opposite result, a higher density of β than α misfit dislocations.[4–6]

A substrate misorientation changes the angle between the stress due to the interfacial misfit strain and the {111} slip planes, increasing or decreasing the resolved shear stress (RSS) on each dislocation slip system. This is illustrated in Fig. 1 for a substrate misorientation towards $(111)A$. Slip systems with a higher RSS will experience a lower activation energy for nucleation[7–9] and a higher glide velocity[10–12] and therefore are expected to dominate nucleation and glide processes. In addition, the higher RSS is predicted to lead to the preferential formation of dislocations with a specific out-of-plane Burger's vector component (tilt component), resulting

a)Electronic mail: rsgold@engin.umich.edu

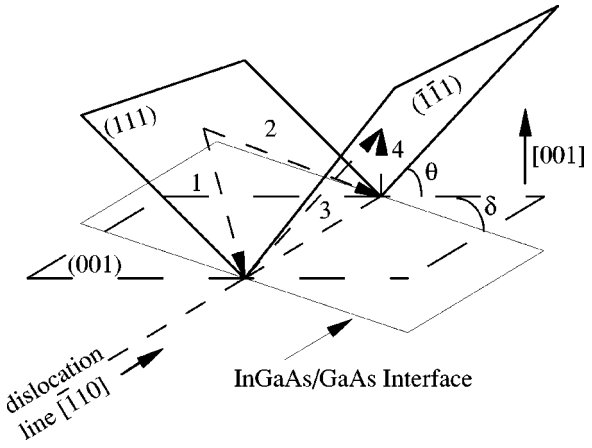

FIG. 1. Perspective of {111} slip planes for an (001) substrate misoriented by δ towards (111)A. The geometry of the Burgers vectors 1–4 are shown for a dislocation with a $[\bar{1}10]$ line direction.

in epilayer tilt.[12] The tilt generated by α and β dislocations will be in proportion to the substrate offcut resolved in the $[110]$ and $[\bar{1}\bar{1}0]$ directions, respectively. Furthermore, the tilt will rotate the epilayer in a direction such that the substrate miscut is reduced, as shown in the schematic of Fig. 2. In most investigations of epilayer tilting in partially relaxed systems, the observations are consistent with the predictions from such RSS analyses. However, the effects of misorientation on the RSS of the α and β slip systems has not been considered explicitly in the literature and limited attention has been paid to the effects of the misorientation *direction* on strain relaxation in general.[9,12]

For a misorientation towards (011), it is evident that the RSS are identical for the α and β slip systems,[13] since the (011) miscut can be decomposed into equal components in the $[\bar{1}\bar{1}0]$ and $[110]$ directions. However, the effect is less obvious for the {111} offcuts. At first glance, it might seem that the (111)A offcut would only change the RSS of the α slip systems and that the (111)B offcut would only change the RSS of the β slip systems. However, since each Burger's vector makes a 60° angle with a $\langle 110 \rangle$ line direction, its position with respect to the interface plane is affected by both (111)A and (111)B misorientations. We show in this article that the number of 60° slip systems with a higher or lower RSS and the magnitude of change in each case are similar for the α and β slip systems, independent of misorientation direction. (In fact, for {111} offcuts, there is an unexpected slightly higher calculated RSS for dislocations with lines perpendicular to the offcut axis. In other words, the RSS of the β and α slip systems are highest for the (111)A and (111)B offcuts, respectively.) Consequently, classical models for dislocation nucleation and glide predict nearly symmetric strain relaxation for all substrate misorientation directions, and epilayer tilt about the offcut axis in a direction such that it reduces the substrate miscut.

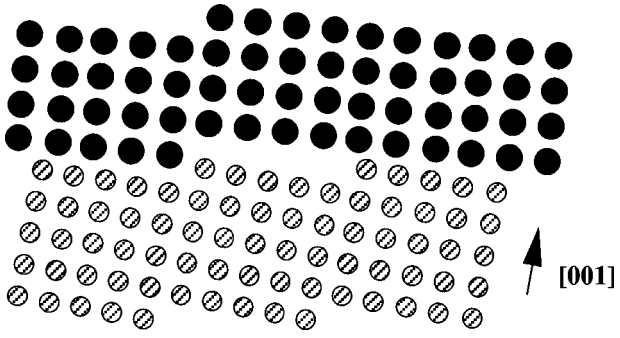

FIG. 2. Schematic of incoherent tilt. The epilayer planes tilt in the direction opposite of the substrate miscut, with the formation of both misfit and tilt dislocations.

We also describe our experimental investigations of the effects of substrate misorientation on strain relaxation in single and multilayer InGaAs-based heterostructures. It will be clear that the predictions based on our RSS calculations for 60° α and β dislocation slip systems cannot explain many of our results. In partially relaxed, single layer InGaAs/GaAs structures, we observe tilt which rotates the epilayer to reduce the substrate misorientation. However, the axis of epilayer tilt varies from the expected alignment with the substrate offcut axis, indicating an asymmetry in epilayer tilt. Also, for the highest growth temperatures investigated, the β tilt is largest for the smallest β substrate offcut. Furthermore, we observe asymmetric relaxation whose polarity (more α or β dislocations) depends on the direction of the substrate offcut. In all cases, the strain relaxation and tilt asymmetries are sensitive to the growth temperature and increase with the magnitude of substrate misorientation. In multilayer InGaAs structures, grown at lower temperatures, the strain relaxation is nearly complete and symmetric. In these structures, epilayer tilt associated with α misfit dislocations decreases the substrate miscut, as expected, while tilt associated with β misfit initially does the same, but as the composition is increased, the tilt unexpectedly reverses direction to *increase* the miscut. The tilt reversal is observed to be correlated with the presence of surface facets. Since these results are not explained by RSS arguments, we consider the role of partial dislocations, dislocation interactions, and surface morphology on the nucleation and glide of 60° dislocations.

The article is organized as follows. In Sec. II we outline calculations of stresses on dislocations due to misfit strain. (The details are given in the Appendix.) Section III describes procedures used for the experimental studies, including molecular beam epitaxial (MBE) growth, high resolution x-ray diffraction, and atomic force microscopy (AFM). In Sec. IV, strain relaxation data and AFM images of surface morphology are presented and discussed. Conclusions are given in Sec. V.

II. RESOLVED SHEAR STRESS CALCULATIONS

For a given slip system, the shear stress due to misfit strain, resolved on the glide plane, in the glide direction, produces a force on a dislocation. The RSS affects both nucleation of dislocation loops and glide of threading dislocations. The activation energy for nucleation is inversely proportional to the RSS,[7–9] and the glide velocity is directly proportional to the RSS.[10,11] There is also evidence that the activation energy for glide is dependent on the RSS.[14] Thus,

TABLE I. Calculated Schmid factors for the eight slip systems of the (001) compressively stressed zincblende semiconductor interface, with 60, 30, and 90° dislocations. Two misorientation directions, (111)A and (011) are tabulated, each with an offcut of 2° [(111)B is a 90° rotation of (111)A]. The Schmid factors for zero offcut are 0.4083, 0.2357, and 0.4714 for 60°, 30°, and 90° dislocations, respectively.

				Misorientation	
Dislocation Line	Burger's Vector	Glide Plane	Tilt Component	(111)A	(011)
$[\bar{1}10]$ (α)	(1) 60° $a/2[10\bar{1}]$	(111)	down	0.4173	0.4220
	30° $a/6[2\bar{1}\bar{1}]$			0.2409	0.2521
	90° $a/6[11\bar{2}]$			0.4819	0.4788
	(2) 60° $a/2[01\bar{1}]$	(111)	down	0.4173	0.4073
	30° $a/6[\bar{1}2\bar{1}]$			0.2409	0.2266
	90° $a/6[11\bar{2}]$			0.4819	0.4788
	(3) 60° $a/2[101]$	$(\bar{1}\bar{1}1)$	up	0.3972	0.3935
	30° $a/6[2\bar{1}1]$			0.2293	0.2193
	90° $a/6[112]$			0.4586	0.4623
	(4) 60° $a/2[011]$	$(\bar{1}\bar{1}1)$	up	0.3972	0.4073
	30° $a/6[\bar{1}21]$			0.2293	0.2431
	90° $a/6[112]$			0.4586	0.4623
$[\bar{1}\bar{1}0]$ (β)	(5) 60° $a/2[\bar{1}0\bar{1}]$	$(\bar{1}\bar{1}1)$	down	0.4178	0.4220
	30° $a/6[\bar{2}1\bar{1}]$			0.2529	0.2521
	90° $a/6[\bar{1}\bar{1}2]$			0.4708	0.4788
	(6) 60° $a/2[01\bar{1}]$	$(\bar{1}\bar{1}1)$	down	0.3977	0.4073
	30° $a/6[12\bar{1}]$			0.2179	0.2266
	90° $a/6[\bar{1}\bar{1}2]$			0.4708	0.4788
	(7) 60° $a/2[\bar{1}01]$	$(1\bar{1}\bar{1})$	up	0.3977	0.3935
	30° $a/6[\bar{2}11]$			0.2179	0.2193
	90° $a/6[\bar{1}12]$			0.4708	0.4623
	(8) 60° $a/2[011]$	$(1\bar{1}\bar{1})$	up	0.4178	0.4073
	30° $a/6[121]$			0.2529	0.2431
	90° $a/6[\bar{1}12]$			0.4708	0.4623

it is expected that the slip system with the greatest RSS will dominate both nucleation and glide processes.

The RSS on each slip system is determined by transforming the stress tensor from the cartesian coordinate system into a new coordinate system where x' corresponds to the glide direction and z' to the glide plane normal.[10] In the general case, the stress tensor in the coordinate system of the slip system is $\sigma'_{ij}=T_{il}T_{jm}\sigma_{lm}$, where σ_{lm} are the applied stresses, and T_{il} and T_{jm} are the matrices which transform the coordinate system of the applied stress to that of the slip system. In this case, a finite stress tensor is generated by the misfit strain at the InGaAs/GaAs interface which produces an in-plane biaxial compressive stress $\sigma=\sigma_{11}=\sigma_{22}$. The component of the stress tensor which corresponds to the stress on the glide plane in the glide direction (the RSS) is equal to $\sigma'_{32}=(T_{31}T_{21}+T_{32}T_{22})\sigma$. The factor in brackets is often called the ''Schmid factor.'' [15]

In zincblende and diamond cubic semiconductors, there are 8 unique 60° $a/2\ \langle 110\rangle\ \{111\}$ slip systems, as listed in Table I. We note that the line direction is chosen to give dislocation slip systems (with the indicated Burger's vector and slip plane) which relieve compressive strain. An equivalent set of 8 slip systems have dislocation lines, Burger's vectors, and slip planes of opposite sign. However, if the sign of the dislocation line is reversed, while the Burger's vector and slip plane remain fixed, the resulting 8 slip systems add strain to a compressively stressed system. We have calculated the Schmid factors for each compressive strain relieving 60° dislocation slip system, and its associated 30 and 90° partial dislocation slip systems, for misorientations towards (011) and (111)A [the RSS for (111)B is a 90° rotation of (111)A]. The details of these calculations are presented in the appendix. Figures 3(a) and 3(b) show plots of the calculated Schmid factor versus offcut angle towards (011) and (111)A, respectively, for the 60° slip systems. Table I lists the numerical values of the Schmid factors for each slip system, for the most common substrate misorientation, 2°. In each case, the Schmid factor of a few of the slip systems increases with offcut angle. These systems will have the highest RSS and therefore are expected to dominate both nucleation and glide processes. In the plot, systems 1–4 and 5–8 are α and β slip systems, respectively.

Considering first 60° dislocations for (011) miscuts, slip systems 1 and 5 have the highest Schmid factors, while 3 and 7 have the lowest Schmid factors. Since 1 and 3 are α dislocations, and 5 and 7 are β dislocations, an equal number of α and β systems with higher or lower Schmid factors are expected, and the relaxation is expected to be isotropic. Furthermore, since systems 1 and 5 both have ''down'' tilt components, nonzero epilayer tilt is expected in both $\langle 110\rangle$ directions, resulting in epilayer tilt about the [010] axis. In other words, for (011) offcuts, RSS arguments predict symmetric relaxation and epilayer tilt about the offcut axis.

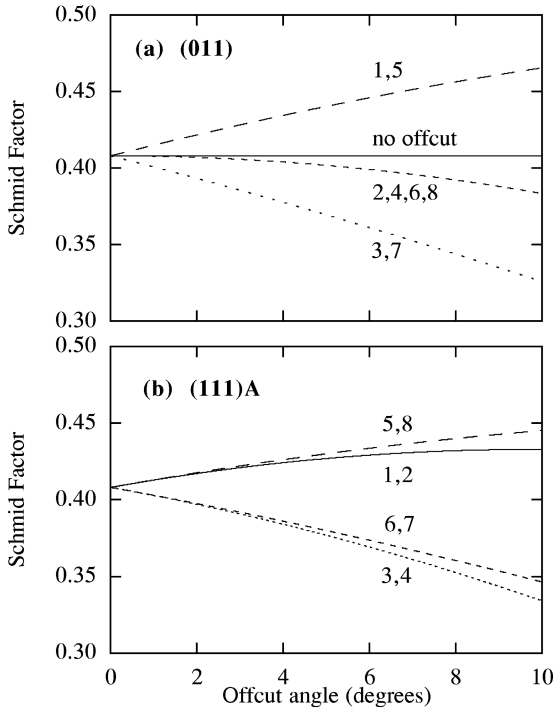

FIG. 3. Schmid factors for 60° dislocation slip systems, as a function of offcut angle towards (a) (011) and (b) (111)*A*. The slip systems are numbered according to the notation used in Tables I–V. Systems 1–4 and 5–8 are α and β dislocations, respectively.

For (111)*A* miscuts, systems 1, 2, 5, and 8 have higher Schmid factors, while 3, 4, 6, and 7 have lower Schmid factors. In fact, systems 5 and 8, which are β dislocations, have slightly higher Schmid factors than systems 1 and 2, which are α dislocations. Thus, for (111)*A* miscuts, β dislocations have a higher Schmid factor than that of the α dislocations. Similarly, for (111)*B* offcuts, α dislocations have a higher Schmid factor than that of the β dislocations.

If nucleation and glide of 60° dislocations is controlled simply by the RSS, the relaxation of strain is expected to occur with a preference for those dislocations with line directions perpendicular to the offcut axis (i.e., β and α dislocations for (111)*A* and (111)*B* offcuts, respectively). Regarding the expected tilt for (111)*A* offcuts, systems 5 and 8 have ''down'' and ''up'' tilt components which cancel each other, resulting in no β epilayer tilt. Meanwhile, systems 1 and 2 both have ''down'' tilt components, resulting in nonzero α epilayer tilt. Similar arguments hold for the (111)*B* miscut, with the directions rotated by 90°, i.e., nonzero β epilayer tilt is expected. Therefore, for {111} offcuts, epilayer tilt about the offcut axis and anisotropic strain relaxation of opposite polarity may be expected for the direct nucleation of 60° dislocations, or for relaxation limited by the glide of 60° dislocations.

We also consider the RSS for partial dislocations. For 30° partials, the β and α dislocations have the highest Schmid factors for (111)*A* and (111)*B* miscuts, respectively. Thus, anisotropic relaxation of opposite polarity may be expected for nucleation dependent on 30° partials. For 90° partials, the situation is reversed—the α and β dislocations have the highest Schmid factors for (111)*A* and (111)*B* miscuts, respectively. Therefore, if the formation of 60° dislocations depends on the nucleation of 90° partial dislocations, as was recently proposed,[16] the strain relaxation would be expected to be anisotropic, with more α and β dislocations for (111)*A* and (111)*B* offcuts, respectively.

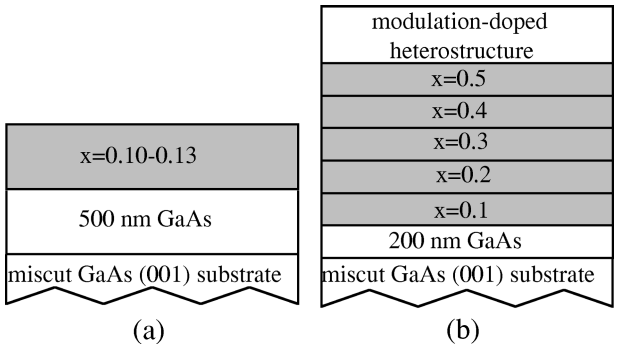

FIG. 4. Cross sections of the targeted layer structures for (a) single $In_xGa_{1-x}As$ layers and (b) compositionally graded $In_xGa_{1-x}As$ multilayer structures.

III. EXPERIMENTAL PROCEDURES

We grew epitaxial InGaAs/GaAs samples by solid-source MBE on semi-insulating (undoped) and *n*-doped ($\sim 2\times10^{18}$ cm^{-3}) GaAs(001) substrates, intentionally misoriented 2–10° towards the (111)*A*, (111)*B*, and (011) planes. The semi-insulating substrates (2° offcut), with etch pit densities $<5\times10^3/cm^2$, were epi-ready (and therefore required no *ex situ* surface preparation), while the *n*-doped substrates (miscut 2–10°), with etch pit densities $<5\times10^2/cm^2$, were etched prior to growth, using $NH_3OH:H_2O_2:H_2O$ (5:2:10) followed by HCl. The GaAs growth rate, set at 0.9 μm/hr, was determined from intensity oscillations of the specular beam of the reflection high energy electron diffraction (RHEED) pattern. The indium fluxes were chosen to yield specific In compositions with As_4/ group III beam equivalent pressure ratios of 35 to 40. The In compositions and layer thicknesses were confirmed by Rutherford backscattering spectrometry. Cross sections of the targeted structures for single layer and multilayer samples are shown in Figs. 4(a) and 4(b), respectively. For the single layer samples, the structures consisted of 200–250 nm Si-doped ($N_d\sim10^{17}$ cm^{-3}) $In_xGa_{1-x}As$ ($0.10\leqslant x\leqslant0.13$) grown on semi-insulating and *n*-doped substrates. The GaAs and InGaAs layers were grown at 580 and 495–535 °C, respectively. The sample thicknesses and In compositions were chosen, based on earlier work, to be above the critical thickness while providing partial strain relaxation.[3] The layers were doped to facilitate cathodoluminescence measurements.[17] The relaxed multilayer samples consisted of a modulation-doped heterostructure grown on a ''stack'' of 5 increasing In composition $In_xGa_{1-x}As$ ($0.10\leqslant x\leqslant0.50$), 200 nm thick, undoped single layers (i.e., a compositionally step-graded buffer), grown on semi-insulating substrates. The GaAs, step-graded buffer, and modulation-doped heterostructure were grown at 580, 350, and 450 °C, respectively. (Since the growth of modulation-doped heterostructure lasted about ten minutes, the step-graded layers were effec-

TABLE II. Summary of strain relaxation data for single $In_xGa_{1-x}As$ ($0.10 \leqslant x \leqslant 0.13$) layers grown in the temperature range 495–535°C. The films grown on semi-insulating and *n*-type substrates had thicknesses of 250 and 200 nm, respectively. Listed are the growth temperature, *T*, the In mole fraction, *x*, the components of the substrate offcut towards the (111)*A* and (111)*B* planes, the strain relaxation with respect to the substrate, *R*, and epilayer tilt, Ω, in both ⟨110⟩ directions.

Growth *T* (°C)	Substrate doping	In Fraction *x*	Substrate Offcut (°)		*R* (%)		Ω (°)	
			(111)*A*	(111)*B*	[110]	[$\bar{1}$10]	[110]	[$\bar{1}$10]
535	S.I.	0.10	0	2.0	55	63	0.08	0.04
		0.10	1.4	1.4	57	43	0.15	0.08
		0.10	2.0	0	47	15	0.15	0.10
515	S.I.	0.12	0	2.0	44	39	0.02	0.13
		0.12	1.4	1.4	63	63	0.21	0.04
		0.12	2.0	0	60	58	0.16	0
495	S.I.	0.13	0	2.0	72	84	0.06	0.10
		0.13	1.4	1.4	85	69	0.17	0.06
		0.13	2.0	0	96	41	0.11	0.03
495	*n*	0.11	2	0	38	35	0.14	0.04
		0.13	4	0	78	59	0.17	0.02
		0.13	6	0	84	57	0.19	0.04
		0.11	8	0	51	32	0.24	0.04
		0.11	10	0	77	23	0.24	0.05
495	*n*	0.12	0	4	44	69	0.003	0.19
		0.13	0	6	54	95	0.03	0.21

tively annealed at 450° for ten minutes.) The 1 μm thick undoped step-graded buffer relaxes the 3.5% lattice-mismatch strain between the GaAs substrate and modulation-doped heterostructure, providing a suitable substrate for optimum electronic properties.[18] At each interface in the step-graded buffer, the mismatch was $\sim$1.5%, similar to the single layer case.

High resolution x-ray diffraction measurements were performed in order to determine the in-plane and out-of-plane *d*-spacings of the films and multilayers, from which the alloy composition, lattice mismatch, and residual strain in the layers were determined. X-ray rocking curves (XRC) of the partially relaxed samples were measured with a double-crystal diffractometer using Cu $K\alpha$ radiation monochromated by a four-reflection Bartels monochromator, which employs Ge(220) reflections in the (+,−,−,+) configuration. Two sets of reflections, the symmetric (004) and the glancing incidence (224) and/or (115) were measured. The (004) rocking curves were recorded at several azimuthal angles to obtain the angle of rotation of the epilayer planes about an in-plane axis (epilayer tilt). In order to determine the in-plane unit cell dimensions, off-axis rocking curves at different azimuthal angles were also measured. In most cases, the (224) reflections were chosen since they are most sensitive to in-plane lattice mismatch.[19] An orthorhombic crystal symmetry was assumed in the analysis. We note that these conventional rocking curve measurements rely on the substrate lattice constant as an internal standard. We have taken extreme care in alignment and centering of the sample in order to eliminate possible samplings of different sample regions during the azimuthal rotation.[20]

For single and multilayer structures, double-crystal x-ray diffraction peaks are significantly broadened due to mosaic tilts associated with relaxation. To resolve the individual steps in the compositionally graded epilayers, triple-axis x-ray measurements were performed at Beamline X18A at the National Synchrotron Light Source (NSLS) at Brookhaven National Laboratory. The wavelength of incident radiation was selected to be 1.653 Å using a double-crystal Si(111) monochromator. The samples were mounted onto a six-circle Huber diffractometer and the signal was collected by a Ge(111) analyzer crystal and scintillation counter. Contour maps were performed near the (004) and (224) Bragg peaks. These contour maps consisted of a series of ω-2θ scans, with the same initial value of 2θ (angle between incident x-ray beam and detector) and a range of initial values of ω (angle between the incident beam and sample). The (004) and (224) *d*-spacings of each epilayer in the multilayer structure were determined from this data. In this case, there is no internal standard needed, and each measurement corresponds to an absolute lattice parameter measurement.[20,21]

AFM measurements of the surfaces of the multilayer structures were undertaken using a Digital Instruments Nanoscope II, in contact mode with a constant net force in the range 30–100 nN, using Si_3N_4 probe tips.

IV. RESULTS AND DISCUSSION

A. Single layers

Table II summarizes the strain relaxation data for single $In_xGa_{1-x}As$ ($0.10 \leqslant x \leqslant 0.13$) layers, grown at 495–535 °C on the semi-insulating (SI) and *n*-doped substrates with various misorientations. The table lists the growth temperature, *T*, the In mole fraction, *x*, components of substrate offcut towards the (111)*A* and (111)*B* planes, the strain relaxation with respect to the substrate, *R*, and epilayer tilt, Ω, in the [110] and [$\bar{1}$10] directions. In each ⟨110⟩ direction, *R* ranged from 35 to 96%, while Ω ranged from 0 to 0.24°. If the interfacial compressive strain relaxes entirely via the misfit (edge) component of 60° dislocations, the misfit dislocation

density in each $\langle 110 \rangle$ direction is $D=(2\sqrt{2}/a)\epsilon$, where ϵ is the relaxed strain, and a is the unstrained epilayer lattice constant. Thus, the calculated linear density of 60° dislocations ranges from 0.25 to 2.0×10^5/cm. This is equivalent to areal dislocation densities ranging from 0.5 to $4.0\times10^5/\text{cm}^2$. However, the etch pit densities of the substrates are $<5\times10^3/\text{cm}^2$, which is 2–3 orders of magnitude less than the density of dislocations required for the measured relaxation. Thus, new dislocations must have formed by nucleation and/or multiplication mechanisms.[16,22–24] For the layers grown on semi-insulating substrates, smaller R is observed for $x=0.10$ and 0.12 in comparison with $x=0.13$, as expected for the lower indium compositions.[4] The layers grown on n-type substrates also follow this trend, although the average R is reduced. This is due in part to a reduced layer thickness (200 nm). It is also possible that the substrate doping and/or surface preparation contribute to the change in magnitude of strain relaxation.

From the magnitude of the tilt angle, Ω, the fraction of 60° dislocations with an out-of-plane Burger's vector in a preferred direction can be calculated using $(2/a)\sin\Omega$, where a is the unstrained epilayer lattice constant. For the highest Ω, 0.24°, 7.35×10^4/cm dislocations, or 49% of the Burger's vectors have a preferred out-of-plane component. In the single layer samples, the tilt rotated the epilayer in a direction such that the substrate miscut was reduced, as expected from RSS models discussed in the previous section.

Asymmetries in R and/or Ω are observed in all of the samples. The $x=0.12$ layers grown at $T=515$ °C on semi-insulating substrates come closest to following the predictions of RSS models. They have symmetric R for all misorientations and the tilt generally increases with offcut angle, except for the α tilt, which is unexpectedly high for the (011) offcut. (Actually, the high α tilt for the (011) offcut occurs for all the growth temperatures investigated.) For growth at $T=535$ °C, the strain relaxation is predominantly symmetric; α tilt increases with offcut angle, but β tilt unexpectedly decreases with offcut angle. Thus, for $T=535$ °C growth, asymmetric relaxation and epilayer tilt do not always occur simultaneously. For example, the $x=0.10$ sample grown on 2° (111)B miscut is more relaxed in the $[\bar{1}10]$ direction (β dislocations), but has larger α tilt. For the lowest growth temperature, $T=495$ °C, the magnitude of strain relaxation and epilayer tilt increase with offcut angle, and a large asymmetry in strain relaxation is observed. For offcuts up to 2°, the strain relaxation asymmetry is largest for (111)A compared with (111)B offcuts. For miscuts greater than 2°, the amount of asymmetry in strain relaxation is roughly equivalent for the (111)A and (111)B miscuts, and increases with misorientation towards both (111)A and (111)B.

These observations, including the fact that a (111)B miscut results in more β relaxation, are not predicted by RSS models, as shown by the calculations in Sec. II and the Appendix. For 60° dislocations, the number of slip systems which have a higher or lower Schmid factor are nearly identical for the α and β slip systems (corresponding to the [110] and $[\bar{1}10]$ relaxation directions). Furthermore, the asymmetric relaxation cannot be explained by intrinsic differences between α and β dislocations,[1,2,13] such as core energies, Peierls barriers contributing to higher glide velocities of α dislocations (in comparison to β dislocations), since in these cases, a higher density of α dislocations, independent of substrate misorientation, would be expected. Since we obtain more β dislocations for (111)B misorientations, alternative explanations must be considered.

As discussed in Sec. II, for 30° and 90° partial dislocations, the number of slip systems which have a higher Schmid factor are not identical for the α and β slip systems. The α and β 90° partial dislocation slip systems have the highest RSS for (111)A and (111)B miscuts, respectively. Therefore, our observations of asymmetric relaxation with higher β relaxation for the (111)B offcut would be predicted by RSS models if relaxation was controlled by the formation of 90° partials. This was also the conclusion in the transmission electron microscopy work of Chen *et al.*[16] If nucleation is controlled by partial dislocation nucleation in diamond cubic semiconductor systems, then similar arguments would predict asymmetric relaxation in SiGe/Si. To our knowledge, asymmetric relaxation in SiGe/Si has not been observed, but studies of {111} offcuts have also not been reported.

In zincblende and diamond cubic semiconductors, 60° dislocations have been observed [with high resolution transmission electron microscopy (TEM)] to be dissociated into 30 and 90° partial dislocations, separated by a stacking fault.[25] The two partial dislocation lines lie parallel to each other on the {111} glide plane, with one below the other with respect to the surface. The relative location of the 30 and 90° partials at the interface depends on the sign of the interfacial strain. In compressively stressed systems such as InGaAs/GaAs(001), the 30° partial dislocation lies furthest from the surface.[16,25] On the other hand, in tensile stressed systems such as Si/GaP(001), the 90° partial is furthest from the surface.[25] In InGaAs/GaAs, the stacking fault width is typically on the order of 5 nm,[26] whereas in Si/GaP, the stacking fault may cover the entire film thickness.[25] These observations suggest that in compressively stressed systems, nucleation of the 30° partial dislocation is quickly followed by nucleation of the 90° partial dislocation, while in tensile stressed systems, nucleation of the 90° partial dislocation occurs first, and is not necessarily followed by nucleation of the 30° partial dislocation. Thus, in a compressively stressed system, it is expected that the rate limiting step for strain relaxation is nucleation of the 30° partial dislocation. On the other hand, if the strain relaxation is limited by nucleation of the 90° partial dislocation, then nucleation of 30° partial dislocations cannot obey the standard stress and temperature dependence. Instead, their formation would be limited by an extrinsic effect occuring during growth, such as the formation of In clusters[6,16] or stress concentrations at step edges.[8]

Several groups have reported correlations between strain relaxation and surface morphology.[4,27,28] The magnitude and direction of GaAs substrate misorientation determine the density and edge termination (Ga or As) of surface and buried interfacial steps. During the growth of GaAs with a (2×4) surface reconstruction, the standard conditions for MBE growth of GaAs, the As-dimers line up along the [110] in-plane direction.[29] Scanning tunneling microscopy studies have indicated that under these conditions, A-type (Ga-

terminated) steps will elongate and smoothen, while *B*-type (As-terminated) steps will become jagged such that locally they consist of both *A*- and *B*-type steps.[29] Previously, for 2° offcuts, we suggested that this local asymmetry in *A*- and *B*-type step edges was correlated with the degree of asymmetric strain relaxation.[4] Our experimental results in this article expand on the number of samples and range of substrate offcuts investigated. In all cases, the trend of increasing asymmetry with offcut towards $(111)A$ and $(111)B$ is evident. These results suggest that the nucleation and/or glide of dislocations in the partially relaxed single layers are influenced by surface or interface step densities. For example, heterogeneous nucleation of dislocations or dislocation multiplication might preferentially occur at step-edges or In clusters associated with steps.[6,30] In addition, glide of dislocations may be facilitated by nucleation of atomic-scale kinks, which would be affected by surface or interface step densities.[11,31]

Note that the average relaxation is similar for samples grown at the same temperature. For example, layers grown at $T=495\,^{\circ}\mathrm{C}$ with an In concentration of 13% have the largest asymmetries, yet a similar average relaxation of $73\pm4\%$. The similar average relaxation might be explained by a dislocation nucleation mechanism that is independent of miscut. If this is true, then the large asymmetries would be explained by glide velocities which are sensitive to misorientation. Therefore, we consider possible mechanisms which are limited by dislocation glide. One possible explanation involves the effect of substrate miscut on the interaction of slip systems. We note that recent computations of dislocation interactions in strained layers indicate negligibile dislocation blocking resulting from dislocation interactions.[32] However, the calculations considered only a diamond cubic semiconductor, SiGe, grown on a singular Si surface. In our case, the different core structures present in III-V compounds and the presence of the miscut may lead to significant effects from interacting dislocations. As mentioned earlier, α dislocations have been reported to have a higher glide velocity than β dislocations in undoped and *n*-type GaAs. If this trend holds in ternary alloys such as InGaAs, α thread segments would be expected to dominate the relaxation process in the samples discussed in this article. Using the Schmid factors tabulated in Table I, we consider the possible impacts of 2° offcuts on relaxation limited by interaction of slip systems. For the $(111)A$ miscut, the two α slip systems with the highest RSS share the same glide plane, (111), while the two β slip systems with highest RSS have different glide planes, $(\bar{1}11)$ and $(1\bar{1}1)$. Since glide of β thread segments can occur on both $(\bar{1}11)$ and $(1\bar{1}1)$, it is possible that the gliding β threads will interact more often than gliding α threads, thereby reducing the amount of glide and the resulting β misfit dislocation length and strain relaxation in the $[\bar{1}10]$ direction. Meanwhile, glide of the α thread segments occurs predominantly on (111); the resulting α misfit dislocation length and strain relaxation in the [110] direction are expected to be greater in this case. As a result, an asymmetry in relaxation would occur with higher α than β relaxation, as observed. Similar arguments hold for $(111)B$ offcuts, with the directions reversed. For (011) offcuts, only one slip system for the α and β systems has the highest RSS (systems 1 and 5). Thus, we include the effects of those slip systems with the second highest Schmid factors: 2,4,6, and 8. Since glide of α thread segments can occur on both (111) and $(\bar{1}\bar{1}1)$, and glide of β thread segments can occur on both $(\bar{1}11)$ and $(1\bar{1}\bar{1})$, it is likely that the gliding α and β thread segments will interact, resulting in reduced glide and misfit dislocation length in both [110] and $[\bar{1}10]$ directions. In this case, asymmetric relaxation might be explained by the reduced velocity of gliding β thread segments in comparison with gliding α thread segments in our *n*-type material.

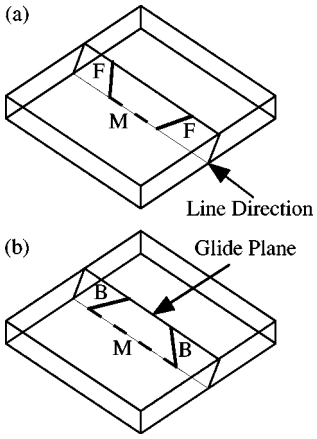

FIG. 5. Schematic representation of (a) forward and (b) backward glide segments. The forward glide, backward glide, and misfit segments are labeled F, B, and M, respectively. For the forward glide segments in (a), one segment has the same character (i.e., α or β) as the misfit segment and the other is a screw segment. In (b), the backward glide segments, one segment has the opposite character as the misfit segment and one is a screw segment.

A second glide-limited mechanism is related to the orientation and type of thread segments associated with misfit dislocations, as shown in Fig. 5. Forward oriented thread segments, shown in Fig. 5(a), have the same character (i.e., α or β) as the misfit segments or are screw segments.[33] Backward oriented thread segments, shown in Fig. 5(b), have the opposite character as the misfit dislocations, or are screw segments. It is possible for β misfit dislocations to form by forward glide of β thread segments or by backwards glide of α thread segments.[34,35] For this mechanism, the forward and backward gliding threads would be subject to the effects of interacting slip systems described in the previous paragraph. In this case, asymmetric relaxation might be explained by a lower velocity of backgliding α thread segments in comparison with forward gliding α thread segments. This mechanism also provides an explanation for the exceptionally high α tilt observed for (011) miscuts at all growth temperatures studied. For the (011) misorientation, the one slip system with the highest RSS (system 1 for α, system 5 for β) probably dominates the initial relaxation process. If forward gliding α thread segments have higher glide velocities than backgliding α thread segments, the resulting α misfit dislocation length and α tilt component are expected to be greatest in this case.

B. Multilayers

We have also investigated strain relaxation in multilayer InGaAs structures grown (at low temperatures) on substrates misoriented by 2° towards (111)*A*, (111)*B*, and (011). The strain relaxation in these structures is nearly complete and symmetric, similar to other step-graded $In_xGa_{1-x}As$ samples grown at this low temperature (350 °C) on nominally flat substrates.[18,36] We note that the growth temperature for these multilayers is significantly lower than that during the growth of the single layers which exhibited asymmetric relaxation ($T=495-515$ °C). Also, in earlier work, step-graded buffers grown in the 495–515 °C temperature range exhibited asymmetric relaxation.[37] At the lower temperatures used for these multilayers, different surface reconstructions[38] and off-stoichiometries[39] which may impact dislocation nucleation often occur. Furthermore, dislocation motion is generally a thermally activated process. Thus, it is likely that the mechanisms of strain relaxation are significantly affected by the growth temperature.

The epilayer tilt results for the multilayer samples grown on offcut substrates have similarities and differences in comparison to other step-graded samples grown (at 350 °C) on nominally flat substrates.[18,36] On one hand, tilt associated with α misfit dislocations always decreases the (111)*A* miscut, as is the case for the other low temperature multilayers. On the other hand, tilt associated with β misfit dislocations initially decreases the (111)*B* miscut, but at the interface between the first and second steps of the buffer, corresponding to In mole fraction >0.2, the tilt reverses direction to increase the miscut again. A similar effect occurs for the single layers grown at 535 °C, where the net β tilt decreases with offcut angle, as was shown in Table II.

Figure 6 shows some of the contour maps from triple-axis x-ray diffraction measurements. In the plots, the *y* axis corresponds to θ, and the *x* axis is ω_{mid}, the center value in each ω-2θ scan. Plotted in this manner, the *y* axis is a measure of *d*-spacing variations, and the *x* axis is a measure of lattice plane tilt. The contours are lines of equal intensity varying from 1000 to 5000 counts/sec, in increments of 1000 counts/sec. The contours displayed were chosen to emphasize the peak positions of all the layers.

The results of the analysis of the data from these multilayer structures are summarized in Table III. The table lists the layer No., In mole fraction *x*, epilayer tilt with respect to the substrate Ω, epilayer tilt with respect to previous layer, Ω_{n-1} (this corresponds to the amount by which the substrate miscut is changed, with the convention that a positive value corresponds to a reduction in offcut), and the effective offcut of the sample. The In compositions in each layer are 0.13, 0.23, 0.32, 0.41, and 0.50 ± 0.01, respectively. Not shown in the table is the strain relaxation, which is nearly complete and symmetric, to within experimental error, in the in-plane ⟨110⟩ directions. In each layer, the strain relaxation with respect to the substrate ranges from 83 to 97 $\pm5\%$ and that with respect to the in-plane lattice constant of the previous layer ranges from 57 to $90\pm5\%$. Thus, the relaxation decreases towards the surface layers, as expected. The overall relaxation of the top epilayer (with respect to the GaAs substrate) is 92%, giving in-plane and out-of-plane surface lattice constants of 5.837 and 5.870 Å, respectively. Assuming that the strain is relaxed by the edge component of 60° dislocations, the linear misfit dislocation density is 1.6×10^6/cm which corresponds to an areal dislocation density of $3.2\times10^6/\mathrm{cm}^2$, distributed among the 5 interfaces. As discussed earlier, the etch pit densities of the substrates are $<5\times10^3/\mathrm{cm}^2$, which is almost 3 orders of magnitude less than the density of dislocations required for the measured relaxation. Thus, at each interface, new dislocations must

TABLE III. Summary of epilayer tilt data for multilayer $In_xGa_{1-x}As$ samples grown at $T=350$ °C on substrates misoriented by 2° towards (111)*A*, (011), and (111)*B*. Listed are the Layer No., indium mole fraction, *x*, epilayer tilt with respect to the substrate, Ω, in both ⟨110⟩ directions, epilayer tilt with respect to the previous layer, Ω_{n-1}, in both ⟨110⟩ directions, and the effective offcut of the substrate.

Layer No.	In Fraction *x*	Ω (°)		Ω_{n-1} (°)		Effective Offcut (°)	
		[110]	[$\bar{1}$10]	[110]	[$\bar{1}$10]	(111)*A*	(111)*B*
(111)*A*							
1	0.12	0.4	0	0.4	0	2.0	0
2	0.23	0.7	0	0.3	0	1.6	0
3	0.32	0.87	0	0.17	0	1.3	0
4	0.41	0.98	0	0.12	0	1.02	0
5	0.50	1.12	0	0.14	0	0.88	0
(011)							
1	0.13	0.19	0.16	0.19	0.16	1.4	1.4
2	0.24	0.29	0.33	0.10	0.17	1.21	1.24
3	0.32	0.31	0.27	0.02	−0.06	1.11	1.07
4	0.40	0.33	0.01	0.02	−0.26	1.09	1.13
5	0.49	0.38	−0.23	0.06	−0.24	1.07	1.39
(111)*B*							
1	0.14	0	0.21	0	0.21	0	2.0
2	0.23	0	0.12	0	−0.09	0	1.79
3	0.32	0	−0.26	0	−0.38	0	1.88
4	0.46	0	−0.40	0	−0.14	0	2.26
5	0.50	0	−0.41	0	−0.01	0	2.4

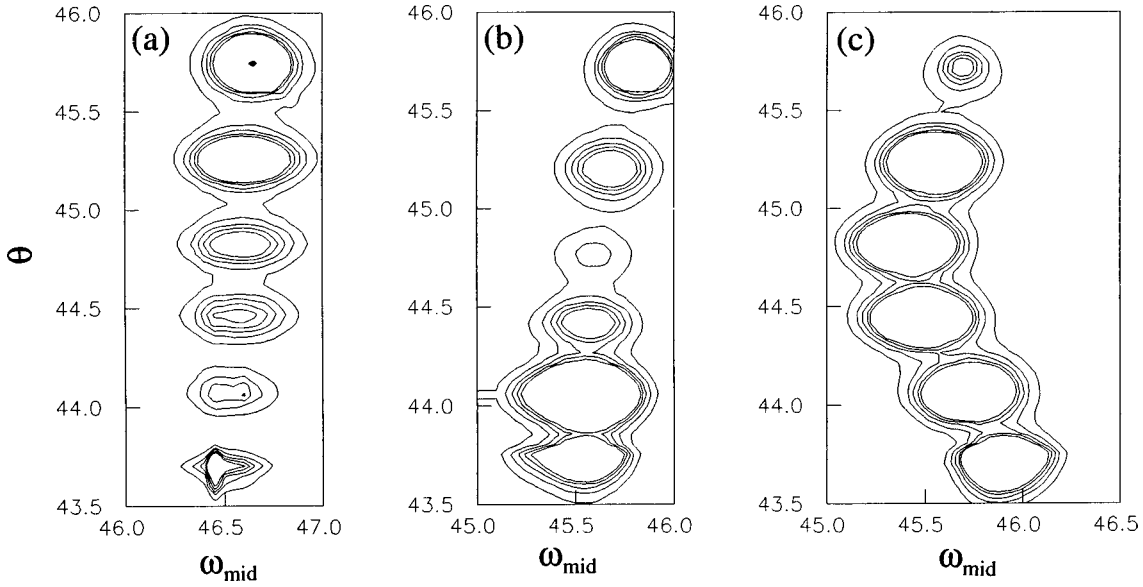

FIG. 6. Triple-axis contour maps, ω_{mid} vs θ_B, performed near the (224) reflection, for nominal offcuts of (a) 0°, (b) 1.4° (111)*A*, and (c) 1.4° (111)*B*, respectively. The maps consist of a series of ω-2θ scans, each with the same initial value of 2θ and a range of initial values of ω. The contours are lines of equal x-ray intensity, varying from 1000 to 5000 counts/s in increments of 1000 counts/s.

have formed by a nucleation and/or multiplication mechanism.[16,22–24]

Figure 6(a) shows a contour map of the 2° (111)*A* misoriented sample, collected with the incident x-ray beam oriented in the $[\bar{1}10]$ direction, for which the offcut is negligible. In the plot, the substrate peak lies at $\theta = 45.739°$, and the 5 steps in the buffer lie at successively smaller θ. The ω_{mid} values of the epilayer peaks are approximately the same as that of the substrate, indicating no measureable tilt in the $[\bar{1}10]$ direction. Similar results were obtained for the 2° (111)*B* offcut sample measured in the [110] direction. In these cases, negligible tilt has occurred when the offcut is negligible, as expected if the offcut provides a driving force to epilayer tilt.

Figure 6(b) shows a contour map of the 2° (011) misoriented sample, collected with the incident x-ray beam aligned in the [110] direction, for which the offcut is 1.4°. In the plot, the ω_{mid} values of the epilayer peaks differ from that of the substrate peak by as much as $+0.38°$, indicating measureable epilayer tilt. Starting from the first epilayer, the $In_xGa_{1-x}As$ layers have tilted 0.19, 0.29, 0.31, 0.33, and 0.38° in the [110] direction. As listed in Table III, the epilayers have tilted such that the [110] miscut is reduced by 0.19, 0.10, 0.02, 0.02, and 0.05°. Similar results were obtained for the 2° (111)*A* offcut, with the incident x-ray beam in [110] direction, for which the offcut is 2° (not shown). In that case, the $In_xGa_{1-x}As$ layers tilted 0.4, 0.7, 0.87, 0.98, and 1.12° in the [110] direction. Furthermore, the tilt observed rotates each epilayer in a direction such that the substrate miscut is reduced by 0.4, 0.3, 0.17, 0.11, and 0.14°. Thus, in both the (011) and (111)*A* offcuts, the tilt in the [110] direction rotates each epilayer such that the [110] direction miscut of the substrate is reduced. The tilt is proportional to the offcut, decreasing as the offcut is reduced, suggesting that the offcut provides a driving force for tilt (as predicted by RSS models).

In Figure 6(c), we present a contour map of the 2° (011) misoriented sample, collected with the incident x-ray beam aligned in the $[\bar{1}10]$ direction, for which the offcut is 1.4°. Here, the differences in the ω_{mid} value range from $+0.33°$ to $-0.56°$, indicating that initially the tilt reduces the miscut, but as the composition increases, the tilt begins to increase the miscut. Starting from the first epilayer, the $In_xGa_{1-x}As$ layers have tilted 0.16, 0.33, 0.27, 0.01, and $-0.23°$ in the $[\bar{1}10]$ direction. Thus, the epilayers have tilted such that the $[\bar{1}10]$ axis miscut is changed by 0.16, 0.17, -0.06, -0.26, and $-0.24°$ (positive/negative values indicate a decrease/increase in offcut). Similar results were obtained for the 2° (111)*B* offcut, with the incident x-ray beam in the $[\bar{1}10]$ direction, for which the offcut is 2° (listed in Table III, but not shown here). Starting from the first layer, the $In_xGa_{1-x}As$ layers have tilted 0.21, 0.12, -0.26, -0.4, and $-0.41°$ in the $[\bar{1}10]$ direction. The epilayers have tilted such that the $[\bar{1}10]$ miscut of the substrate is changed by 0.21, -0.09, -0.38, -0.14, and $-0.01°$. In both cases, the negative Ω_{n-1} values, beginning with the second or third epilayer, are an indication that the tilt has switched directions—at those interfaces the β miscut has increased! We note that an increase in β offcut was also observed for the single layers grown at the highest temperature, $T = 535$ °C. This result—*reverse tilt*—is completely inconsistent with the idea of the substrate offcut providing a driving force for the tilt. It is possible that the substrate initially contained an unequal distribution of Burger's vector components which influenced the distribution of dislocations produced by a multiplicative source. However, since the change in tilt direction occurs at layer Nos. 2 or 3, it is unlikely that

the original substrate dislocations are still influencing the distribution of dislocations.

It is interesting to note that the increase in miscut in the $[\bar{1}10]$ direction (β tilt) occurs after layer No. 2 in both the $(111)B$ and (011) misoriented samples. It is possible that a rough surface morphology of layers Nos. 2 or 3 led to a change in the mechanism of strain relaxation. Nomarski interference micrographs indicate that the cross hatches[40,41] on the final surfaces of the $(111)B$ and (011) misoriented multilayer samples are roughened in comparison with those observed on the surface of the $(111)A$ misoriented sample. This may be an indication of differences in the morphologies at the buried interfaces. In addition, atomic force microscopy indicates the presence of facets with slopes $>2°$ on the surface of the $(111)B$ and (011) misoriented samples.

Figure 7 shows atomic force microscopy images of the surfaces of the $(111)A$ and $(111)B$ misoriented samples. The $0.5\ \mu m \times 0.5\ \mu m$ images in (a) and (b) correspond to the $(111)A$ and $(111)B$ misoriented samples, respectively. In (a), a cross-hatch trough (typical of this surface),[40,41] is clearly visible. For the $(111)B$ misoriented sample shown in (b), cross-hatch troughs are not apparent; instead, the surface contains large facets aligned along [110] directions. The most prominent facet in (b) has sides with 3–6° slopes in the $[\bar{1}10]$ direction. The higher resolution views ($0.2\ \mu m \times 0.2\ \mu m$) shown in (c) and (d) for the $(111)A$ and $(111)B$ misoriented samples emphasize the differences in morphology of these samples. For the $(111)A$ misorientation, shown in (c), the small-lengthscale roughness observed is isotropic. On the other hand, for the $(111)B$ misorientation, shown in (d), the surface morphology is dominated by the $\langle 110 \rangle$ oriented facets. The surface facets generate local offcuts in the $[\bar{1}10]$ direction which are comparable to or larger than the macroscopic $[\bar{1}10]$ substrate offcut. Thus, the facets, presumably induced by strain-induced surface diffusion, may provide a driving force for the observed reversal in β epilayer tilt which finally increases the macroscopic miscut. A similar surface-mediated effect may be occurring in the single layer samples grown at 535 °C.

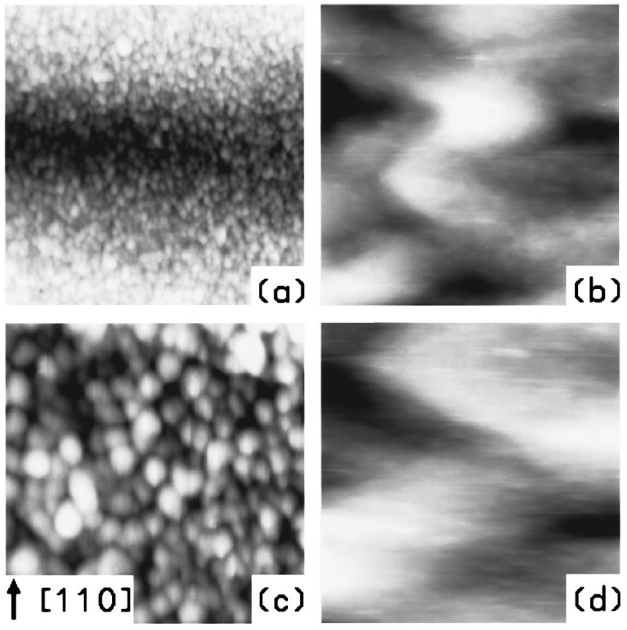

FIG. 7. Atomic force micrographs of the surfaces of the multilayers grown on $(111)A$ and $(111)B$ misoriented substrates. (a) and (b) are $0.5 \times 0.5\ \mu m$ images of $(111)A$ and $(111)B$ misorientations. (c) and (d) are $0.2 \times 0.2\ \mu m$ images of $(111)A$ and $(111)B$ misorientations. The grey-scale ranges displayed are 234, 108, 97, and 71 Å, for (a)–(d), respectively.

V. CONCLUSIONS

In summary, we have investigated the effects of substrate misorientation on strain relaxation in $In_xGa_{1-x}As$/GaAs heterostructures. Our calculations of Schmid factors indicate similar dislocation activation energies and glide velocities for 60° α and β dislocation slip systems, but unequal Schmid factors for 30 and 90° α and β partial dislocation slip systems. Thus, classical models for 60° dislocation nucleation and glide predict that α and β slip systems have similar activation energies for dislocation nucleation and similar glide velocities. These models also predict that epilayer tilt will reduce the substrate miscut. However, measurements of single $In_xGa_{1-x}As$ ($0.10 \leqslant x \leqslant 0.13$) layers, grown at $T \leqslant 515$ °C, reveal asymmetries in strain relaxation which depend on the substrate misorientation direction and magnitude. The direction of highest strain relaxation can be controlled by the direction of substrate misorientation, while the percent of strain relaxation asymmetry can be controlled by the magnitude of substrate misorientation. In symmetrically relaxed multilayer structures (grown at 350 °C and annealed for ten minutes at 450 °C), epilayer tilt which increases the $(111)B$ miscut (i.e., *reverse tilt*) is observed to be correlated with the presence of micron-scale facets presumably arising from strain-induced surface diffusion. This *reverse tilt* is also observed in single layers grown at higher temperatures (535 °C). We discuss possible nucleation and/or glide-limited mechanisms for asymmetric relaxation in lattice-mismatched zincblende semiconductor systems. These include nucleation limited by 90° partial dislocations, glide limited by interacting thread segments, and a mechanism based on the formation of α and β misfit dislocations by forward and backward gliding α thread segments, respectively. These results suggest that local surface or interface step morphologies are more important than bulk stress effects in determining dislocation nucleation and glide in the InGaAs/GaAs system. Further work is needed in order to fully understand the interplay between growth conditions, dislocation nucleation, and strain relaxation in lattice-mismatched semiconductor films and heterostructures.

ACKNOWLEDGMENTS

The authors thank C. Palmstrøm for providing the high offcut substrates. This research was supported in part by the National Science Foundation Grant No. PYI-DMR-9157724 and the Office of Naval Research (ONR) Grant No. N00014-89-J-1147. One of the authors (R.S.G.) acknowledges support of the ONR through an AASERT Fellowship while at UCSD, and the support of the Dow Corning Foundation since arriving at U-M. The National Synchrotron Light Source (NSLS) is supported by the Department of Energy

(DOE) Grant No. DE-AC02-76H0016. S.N.E. and Beamline X18A of the NSLS are supported by DOE Grant No. DE-FG02-85ER4518. K.L.K. and R.S.G. also acknowledge travel support from the NSLS Faculty-Student Research Support Program.

APPENDIX A

In III-V compounds, there are eight possible 60° dislocation slip systems. In addition, the 60° dislocations can dissociate into 30 and 90° partial dislocations, which may play a role in dislocation nucleation in the InGaAs/GaAs system.[16] Thus, a total of 24 slip systems are possible. In this appendix, we present calculations of the RSS on these slip systems for substrate misorientations towards (011) and (111)*A* [the RSS for (111)*B* is a 90° rotation of (111)*A*]. For these calculations, several coordinate system transformations were implemented, using the following transformation matrix:[42]

$$\begin{bmatrix} i\cdot i' & j\cdot i' & k\cdot i' \\ i\cdot j' & j\cdot j' & k\cdot j' \\ i\cdot k' & j\cdot k' & k\cdot k' \end{bmatrix}, \tag{A1}$$

where $(i,j,k)=(x_1,x_2,x_3)$, the initial coordinate system, and $(i',j',k')=(x_1',x_2',x_3')$, the final coordinate system. Section A1 presents the matrices which transform the Cartesian coordinate system to the coordinate system for each slip system. In Secs. A2 and A3, for the (011) and (111)*A* offcuts, the misfit stress at the interface is resolved onto the (001) plane, in the Cartesian coordinate system. The stress tensor is then resolved on the glide plane in the glide direction for each slip system, using the calculated transformation matrices.

A1. Cartesian-slip system transformation

Table IV summarizes the coordinate systems for each of the 24 slip systems. Using Eq. (A1), the matrices which transform the Cartesian coordinate system to the slip system coordinate system are composed of rows of the coordinate system vectors, as follows:

$$T_{ij}=\begin{bmatrix} x_1 \\ x_2 \\ x_3 \end{bmatrix}. \tag{A2}$$

As an example, the matrix which transforms the Cartesian system to the 60° $a/2[10\bar{1}]$ (111) slip system is shown in Eq. (A3):

$$T_{ij}=\begin{bmatrix} -1/\sqrt{6} & -2/\sqrt{6} & -1/\sqrt{6} \\ 1/\sqrt{6} & 0 & -1/\sqrt{2} \\ 1/\sqrt{3} & 1/\sqrt{3} & 1/\sqrt{3} \end{bmatrix}. \tag{A3}$$

A2. (011) Misorientation

For the (011) offcut, the first transformation performed rotates the surface normal back to (001). As shown in Fig. 8,

TABLE IV. Summary of the coordinate systems, (x_1,x_2,x_3), for the eight possible slip systems with 60, 30, and 90° dislocations.

Dislocation Line	Burger's Vector	Glide Plane	x_1	x_2	x_3
$[\bar{1}10]$ (α)	(1) 60° $a/2[10\bar{1}]$	(111)	$a/\sqrt{6}[\bar{1}2\bar{1}]$	$a/\sqrt{2}[10\bar{1}]$	$a/\sqrt{3}[111]$
	30° $a/6[2\bar{1}1]$		$a/\sqrt{2}[0\bar{1}1]$	$a/\sqrt{6}[2\bar{1}1]$	$a/\sqrt{3}[111]$
	90° $a/6[11\bar{2}]$		$a/\sqrt{2}[\bar{1}10]$	$a/\sqrt{6}[11\bar{2}]$	$a/\sqrt{3}[111]$
	(2) 60° $a/2[01\bar{1}]$	(111)	$a/\sqrt{6}[2\bar{1}1]$	$a/\sqrt{2}[01\bar{1}]$	$a/\sqrt{3}[111]$
	30° $a/6[\bar{1}2\bar{1}]$		$a/\sqrt{2}[10\bar{1}]$	$a/\sqrt{6}[\bar{1}2\bar{1}]$	$a/\sqrt{3}[111]$
	90° $a/6[11\bar{2}]$		$a/\sqrt{2}[\bar{1}10]$	$a/\sqrt{6}[11\bar{2}]$	$a/\sqrt{3}[111]$
	(3) 60° $a/2[101]$	$(\bar{1}\bar{1}1)$	$a/\sqrt{6}[\bar{1}2\bar{1}]$	$a/\sqrt{2}[101]$	$a/\sqrt{3}[\bar{1}\bar{1}1]$
	30° $a/6[2\bar{1}\bar{1}]$		$a/\sqrt{2}[011]$	$a/\sqrt{6}[2\bar{1}\bar{1}]$	$a/\sqrt{3}[\bar{1}\bar{1}1]$
	90° $a/6[112]$		$a/\sqrt{2}[\bar{1}10]$	$a/\sqrt{6}[112]$	$a/\sqrt{3}[\bar{1}\bar{1}1]$
	(4) 60° $a/2[011]$	$(\bar{1}\bar{1}1)$	$a/\sqrt{6}[\bar{2}1\bar{1}]$	$a/\sqrt{2}[011]$	$a/\sqrt{3}[\bar{1}\bar{1}1]$
	30° $a/6[\bar{1}21]$		$a/\sqrt{2}[\bar{1}01]$	$a/\sqrt{6}[\bar{1}21]$	$a/\sqrt{3}[\bar{1}\bar{1}1]$
	90° $a/6[112]$		$a/\sqrt{2}[\bar{1}10]$	$a/\sqrt{6}[112]$	$a/\sqrt{3}[111]$
$[\bar{1}\bar{1}0]$ (β)	(5) 60° $a/2[\bar{1}01]$	$(\bar{1}\bar{1}1)$	$a/\sqrt{6}[\bar{1}21]$	$a/\sqrt{2}[\bar{1}01]$	$a/\sqrt{3}[\bar{1}\bar{1}1]$
	30° $a/6[\bar{2}11]$		$a/\sqrt{2}[0\bar{1}1]$	$a/\sqrt{6}[\bar{2}11]$	$a/\sqrt{3}[\bar{1}\bar{1}1]$
	90° $a/6[\bar{1}\bar{1}2]$		$a/\sqrt{2}[\bar{1}10]$	$a/\sqrt{6}[\bar{1}\bar{1}2]$	$a/\sqrt{3}[\bar{1}\bar{1}1]$
	(6) 60° $a/2[011]$	$(\bar{1}\bar{1}1)$	$a/\sqrt{6}[211]$	$a/\sqrt{2}[011]$	$a/\sqrt{3}[\bar{1}\bar{1}1]$
	30° $a/6[12\bar{1}]$		$a/\sqrt{2}[\bar{1}01]$	$a/\sqrt{6}[12\bar{1}]$	$a/\sqrt{3}[\bar{1}\bar{1}1]$
	90° $a/6[\bar{1}\bar{1}2]$		$a/\sqrt{2}[\bar{1}10]$	$a/\sqrt{6}[\bar{1}\bar{1}2]$	$a/\sqrt{3}[\bar{1}\bar{1}1]$
	(7) 60° $a/2[\bar{1}01]$	$(1\bar{1}\bar{1})$	$a/\sqrt{6}[\bar{1}21]$	$a/\sqrt{2}[\bar{1}01]$	$a/\sqrt{3}[1\bar{1}\bar{1}]$
	30° $a/6[\bar{2}11]$		$a/\sqrt{2}[011]$	$a/\sqrt{6}[\bar{2}11]$	$a/\sqrt{3}[1\bar{1}\bar{1}]$
	90° $a/6[\bar{1}12]$		$a/\sqrt{2}[\bar{1}10]$	$a/\sqrt{6}[\bar{1}12]$	$a/\sqrt{3}[1\bar{1}\bar{1}]$
	(8) 60° $a/2[011]$	$(1\bar{1}\bar{1})$	$a/\sqrt{6}[\bar{2}11]$	$a/\sqrt{2}[011]$	$a/\sqrt{3}[1\bar{1}\bar{1}]$
	30° $a/6[121]$		$a/\sqrt{2}[\bar{1}01]$	$a/\sqrt{6}[121]$	$a/\sqrt{3}[1\bar{1}\bar{1}]$
	90° $a/6[\bar{1}12]$		$a/\sqrt{2}[\bar{1}10]$	$a/\sqrt{6}[\bar{1}12]$	$a/\sqrt{3}[1\bar{1}\bar{1}]$

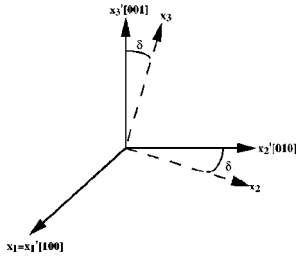

FIG. 8. Illustration of coordinate transformation for the (011) misoriented substrate, which rotates the surface normal back to (001). The coordinate system ([100],[010]-δ,[001]-δ) is transformed to ([100],[010],[001]).

the coordinate system ([100],[010]-δ,[001]-δ) is transformed to ([100],[010],[001]), using the matrix (A4):

$$T_{ij}=\begin{bmatrix} 1 & 0 & 0 \\ 0 & \cos\delta & \sin\delta \\ 0 & -\sin\delta & \cos\delta \end{bmatrix}. \tag{A4}$$

Using the transformation matrix (A4), the interfacial biaxial compressive stress $\sigma=\sigma_{11}=\sigma_{22}$, is resolved onto the (001) plane by the expression, $\sigma'_{ij}=T_{il}T_{jm}\sigma_{lm}$. Thus, the stress on the (001) plane, in the cartesian coordinate system becomes:

$$\sigma'=\sigma\begin{bmatrix} 1 & 0 & 0 \\ 0 & \cos^2\delta & -\sin\delta\cos\delta \\ 0 & -\sin\delta\cos\delta & \sin^2\delta \end{bmatrix}. \tag{A5}$$

Finally, the stress tensor in (A5) is resolved into each particular slip system, using the expression, $\sigma''_{ij}=T_{il}T_{jm}\sigma'_{lm}$.[10] The stress component which corresponds to the stress on the glide plane in the glide direction, or resolved shear stress, is σ''_{32}, which becomes:

$$\sigma''_{32}=(T_{31}T_{21}+T_{32}T_{22}\cos^2\delta-(T_{32}T_{23}+T_{33}T_{22})\sin\delta\cos\delta+T_{33}T_{23}\sin^2\delta)\sigma. \tag{A6}$$

Using Table IV and Eq. (A6), the resolved shear stresses are calculated for each slip system, leading to results similar to previous calculations.[13] The factors preceeding σ, the Schmid factors, are summarized in Table V.

A3. (111)*A* misorientation

For the (111)*A* offcut, two transformations are performed. The first transformation, shown in Fig. 9(a), rotates the surface normal back to (001). The coordinate system ([110]-δ,[$\bar{1}$10],[001]-δ) is transformed to ([110],[$\bar{1}$10],[001]) using the matrix (A7):

$$T_{ij}=\begin{bmatrix} \cos\delta & 0 & \sin\delta \\ 0 & 1 & 0 \\ \sin\delta & 0 & \cos\delta \end{bmatrix} \tag{A7}$$

and the stress on the (001) plane, in the ([110],[$\bar{1}$10],[001]) coordinate system becomes:

TABLE V. Calculated Schmid factors for the eight slip systems with 60, 30, and 90° dislocations. The substrate is misoriented by δ towards (111)*A* or (011) ((111)*B* is a 90° rotation of (111)*A*.

Dislocation Line	Burger's Vector	Glide Plane	Tilt Component	Schmid factor (111)*A*	Schmid factor (011)
[$\bar{1}$10] (α)	(1) 60° $a/2[10\bar{1}]$	(111)	down	$1/\sqrt{6}[\cos^2\delta+(1/\sqrt{2})\sin\delta\cos\delta-\sin^2\delta]$	$1/\sqrt{6}[\cos^2\delta+\sin\delta\cos\delta]$
	30° $a/6[2\bar{1}\bar{1}]$			$1/\sqrt{18}[\cos^2\delta+(1/\sqrt{2})\sin\delta\cos\delta-\sin^2\delta]$	$1/\sqrt{18}[1+2\sin\delta\cos\delta]$
	90° $a/6[11\bar{2}]$			$2/\sqrt{18}[\cos^2\delta+(1/\sqrt{2})\sin\delta\cos\delta-\sin^2\delta]$	$1/\sqrt{18}[2\cos^2\delta+\sin\delta\cos\delta-\sin^2\delta]$
	(2) 60° $a/2[01\bar{1}]$	(111)	down	$1/\sqrt{6}[\cos^2\delta+(1/\sqrt{2})\sin\delta\cos\delta-\sin^2\delta]$	$1/\sqrt{6}[\cos^2\delta-\sin^2\delta]$
	30° $a/6[\bar{1}2\bar{1}]$			$1/\sqrt{18}[\cos^2\delta+(1/\sqrt{2})\sin\delta\cos\delta-\sin^2\delta]$	$1/\sqrt{18}[\cos^2\delta-\sin\delta\cos\delta-2\sin^2\delta]$
	90° $a/6[11\bar{2}]$			$2/\sqrt{18}[\cos^2\delta+(1/\sqrt{2})\sin\delta\cos\delta-\sin^2\delta]$	$1/\sqrt{18}[2\cos^2\delta+\sin\delta\cos\delta-\sin^2\delta]$
	(3) 60° $a/2[101]$	($\bar{1}\bar{1}$1)	up	$1/\sqrt{6}[\sin^2\delta+(1/\sqrt{2})\sin\delta\cos\delta-\cos^2\delta]$	$1/\sqrt{6}[\sin\delta\cos\delta-\cos^2\delta]$
	30° $a/6[2\bar{1}\bar{1}]$			$1/\sqrt{18}[\sin^2\delta+(1/\sqrt{2})\sin\delta\cos\delta-\cos^2\delta]$	$1/\sqrt{18}[2\sin\delta\cos\delta-1]$
	90° $a/6[112]$			$2/\sqrt{18}[\sin^2\delta+(1/\sqrt{2})\sin\delta\cos\delta-\cos^2\delta]$	$1/\sqrt{18}[\sin^2\delta+\sin\delta\cos\delta-2\cos^2\delta]$
	(4) 60° $a/2[011]$	($\bar{1}\bar{1}$1)	up	$1/\sqrt{6}[\sin^2\delta+(1/\sqrt{2})\sin\delta\cos\delta-\cos^2\delta]$	$1/\sqrt{6}[\sin^2\delta-\cos^2\delta]$
	30° $a/6[\bar{1}21]$			$1/\sqrt{18}[\sin^2\delta+(1/\sqrt{2})\sin\delta\cos\delta-\cos^2\delta]$	$1/\sqrt{18}[2\sin^2\delta-\sin\delta\cos\delta-\cos^2\delta]$
	90° $a/6[112]$			$2/\sqrt{18}[\sin^2\delta+(1/\sqrt{2})\sin\delta\cos\delta-\cos^2\delta]$	$1/\sqrt{18}[\sin^2\delta+\sin\delta\cos\delta-2\cos^2\delta]$
[$\bar{1}\bar{1}$0] (β)	(5) 60° $a/2[\bar{1}0\bar{1}]$	($\bar{1}$11)	down	$1/\sqrt{6}[\cos^2\delta+(1/\sqrt{2})\sin\delta\cos\delta]$	$1/\sqrt{6}[\cos^2\delta+\sin\delta\cos\delta]$
	30° $a/6[\bar{2}11]$			$1/\sqrt{18}[\cos^2\delta+(3/\sqrt{2})\sin\delta\cos\delta]$	$1/\sqrt{18}[1+2\sin\delta\cos\delta]$
	90° $a/6[\bar{1}\bar{1}2]$			$-2/\sqrt{18}[\cos^2\delta]$	$1/\sqrt{18}[2\cos^2\delta+\sin\delta\cos\delta-\sin^2\delta]$
	(6) 60° $a/2[01\bar{1}]$	($\bar{1}$11)	down	$1/\sqrt{6}[\cos^2\delta+(1/\sqrt{2})\sin\delta\cos\delta]$	$1/\sqrt{6}[\cos^2\delta-\sin^2\delta]$
	30° $a/6[12\bar{1}]$			$1/\sqrt{18}[\cos^2\delta-(3/\sqrt{2})\sin\delta\cos\delta]$	$1/\sqrt{18}[\cos^2\delta-\sin\delta\cos\delta-2\sin^2\delta]$
	90° $a/6[\bar{1}\bar{1}2]$			$-2/\sqrt{18}[\cos^2\delta]$	$1/\sqrt{18}[2\cos^2\delta+\sin\delta\cos\delta-\sin^2\delta]$
	(7) 60° $a/2[\bar{1}01]$	(1$\bar{1}$1)	up	$1/\sqrt{6}[(1/\sqrt{2})\sin\delta\cos\delta-\cos^2\delta]$	$1/\sqrt{6}[\sin\delta\cos\delta-\cos^2\delta]$
	30° $a/6[\bar{2}11]$			$1/\sqrt{18}[(3/\sqrt{2})\sin\delta\cos\delta-\cos^2\delta]$	$1/\sqrt{18}[2\sin\delta\cos\delta-c1]$
	90° $a/6[\bar{1}12]$			$2/\sqrt{18}[\cos^2\delta]$	$2/\sqrt{18}[\sin^2\delta+\sin\delta\cos\delta-2\cos^2\delta]$
	(8) 60° $a/2[011]$	(1$\bar{1}$1)	up	$-1/\sqrt{6}[(1/\sqrt{2})\sin\delta\cos\delta-\cos^2\delta]$	$1/\sqrt{6}[\sin^2\delta-\cos^2\delta]$
	30° $a/6[121]$			$-1/\sqrt{18}[\cos^2\delta+(3/\sqrt{2})\sin\delta\cos\delta]$	$-1/\sqrt{18}[2\sin^2\delta-\sin\delta\cos\delta-\cos^2\delta]$
	90° $a/6[\bar{1}12]$			$2/\sqrt{18}[\cos^2\delta]$	$2/\sqrt{18}[\sin^2\delta+\sin\delta\cos\delta-2\cos^2\delta]$

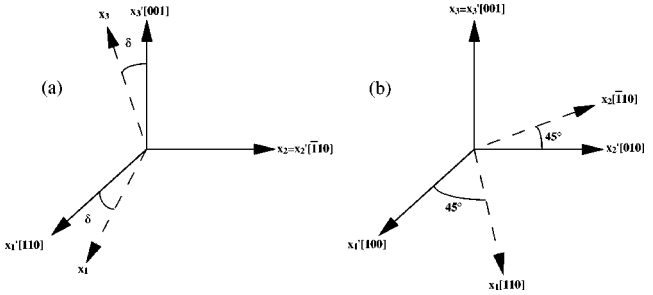

FIG. 9. Illustration of coordinate system transformations for the (111)*A* misoriented substrate, which (a) rotates the surface normal back to (001) and (b) rotates the coordinate system into the Cartesian system. In (a) the coordinate system ($[110]$-δ,$[\bar{1}10]$,$[001]$-δ) is transformed to ($[110]$,$[\bar{1}10]$,$[001]$). In (b) the coordinate system ($[110]$,$[\bar{1}10]$,$[001]$) is transformed to ($[100]$,$[010]$,$[001]$).

$$\sigma' = \sigma \begin{bmatrix} \cos^2\delta & 0 & -\sin\delta\cos\delta \\ 0 & 1 & 0 \\ -\sin\delta\cos\delta & 0 & \sin^2\delta \end{bmatrix}. \tag{A8}$$

In the second transformation, shown in Fig. 9(b), the ($[110]$,$[\bar{1}10]$,$[001]$) coordinate system is transformed to the Cartesian coordinate system, ($[100]$,$[010]$,$[001]$) using matrix (A9):

$$T_{ij} = \begin{bmatrix} -1/\sqrt{2} & -1/\sqrt{2} & 0 \\ 1/\sqrt{2} & 1/\sqrt{2} & 0 \\ 0 & 0 & 1 \end{bmatrix} \tag{A9}$$

and the stress on the (001) plane, in the Cartesian coordinate system becomes:

$$\begin{bmatrix} 1/2(\cos^2\delta+1) & 1/2(\cos^2\delta-1) & -1/\sqrt{2}(\sin\delta\cos\delta) \\ 1/2(\cos^2\delta-1) & 1/2(\cos^2\delta+1) & -1/\sqrt{2}(\sin\delta\cos\delta) \\ -1/\sqrt{2}(\sin\delta\cos\delta) & -1/\sqrt{2}(\sin\delta\cos\delta) & \sin^2\delta \end{bmatrix}. \tag{A10}$$

Finally, the stress tensor in A10 is resolved into each slip system, using the expression $\sigma'''_{ij} = T_{il}T_{jm}\sigma''_{lm}$. The resolved shear stress is σ'''_{32}, which becomes:

$$\begin{aligned}\sigma'''_{32} = \{&1/2(\cos^2\delta+1)[T_{31}T_{21}+T_{32}T_{22}]+1/2(\cos^2\delta \\ &-1)[T_{31}T_{22}+T_{32}T_{21}]-1/\sqrt{2}(\sin\delta\cos\delta)[T_{31}T_{23} \\ &+T_{32}T_{23}+T_{33}T_{21}+T_{33}T_{22}]+\sin^2\delta T_{33}T_{23}\}\sigma.\end{aligned} \tag{A11}$$

Using Table IV and Eq. (A11), the resolved shear stresses are calculated for each slip system, and the resulting Schmid factors are summarized in Table V.

[1] H. Steinhardt and P. Haasen, Phys. Status Solidi A **49**, 93 (1978).
[2] I. Yonenaga and K. Sumino, J. Cryst. Growth **126**, 19 (1993).
[3] K. L. Kavanagh, M. A. Capano, L. W. Hobbs, J. C. Barbour, P. M. J. Maree, W. Schaff, J. W. Mayer, D. Pettit, J. M. Woodall, J. A. Stroscio, and R. M. Feenstra, J. Appl. Phys. **64**, 4843 (1988).
[4] R. S. Goldman, H. H. Wieder, and K. L. Kavanagh, Appl. Phys. Lett. **67**, 344 (1995).
[5] P. Maigne and A. P. Roth, Appl. Phys. Lett. **62**, 873 (1993).
[6] P. Werner, N. D. Zakharov, Y. Chen, Z. Liliental-Weber, J. Washburn, J. F. Klem, and J. Y. Tsao, Appl. Phys. Lett. **62**, 2798 (1993).
[7] S. V. Kamat and J. P. Hirth, J. Appl. Phys. **67**, 6844 (1990).
[8] J. P. Hirth and A. G. Evans, J. Appl. Phys. **60**, 2372 (1986).
[9] P. M. Mooney, F. K. LeGoues, J. Tersoff, and J. O. Chu, J. Appl. Phys. **75**, 3968 (1994).
[10] J. P. Hirth and J. Lothe, in *Theory of Dislocations* (Wiley, New York, 1982), p. 287.
[11] R. Hull and J. C. Bean, Crit. Rev. Solid State Mater. Sci. **17**, 507 (1992).
[12] J. E. Ayers, S. K. Ghandhi, and L. J. Schowalter, J. Cryst. Growth **113**, 430 (1991).
[13] B. A. Fox and W. A. Jesser, J. Appl. Phys. **68**, 2739 (1990).
[14] R. Hull, J. C. Bean, and C. Buescher, J. Appl. Phys. **66**, 5837 (1989).
[15] E. Schmid, Z. Elecktrochem. **37**, 447 (1931).
[16] Y. Chen, Z. Liliental-Weber, J. Washburn, J. F. Klem, and J. Y. Tsao, Appl. Phys. Lett. **66**, 499 (1995).
[17] D. H. Rich, K. Rammohan, Y. Tan, H. T. Lin, R. S. Goldman, K. L. Kavanagh, and H. H. Wieder, J. Vac. Sci. Technol. B **13**, 1766 (1995).
[18] R. S. Goldman, K. L. Kavanagh, H. H. Wieder, and S. N. Ehrlich, J. Vac. Sci. Technol. B **14**, 3035 (1996).
[19] M. A. G. Halliwell, Adv. X-Ray Anal. **33**, 61 (1990).
[20] P. F. Fewster and N. L. Andrew, J. Appl. Crystallogr. **28**, 451 (1995).
[21] P. F. Fewster, Crit. Rev. Solid State Mater. Sci. **22**, 69 (1997).
[22] D. D. Perovic and D. C. Houghton, Phys. Status Solidi A **138**, 425 (1993).
[23] F. K. LeGoues, K. Eberl, and S. S. Iyer, Appl. Phys. Lett. **60**, 23 (1992).
[24] A. Lefebvre and C. Ulhaq-Bouillet, Philos. Mag. A **70**, 999 (1994).
[25] P. M. J. Maree, J. C. Barbour, J. F. van der Veen, K. L. Kavanagh, C. W. T. Bulle-Lieuwma, and M. P. A. Viegers, J. Appl. Phys. **62**, 4413 (1987).
[26] Y. Chen, N. D. Zakharov, P. Werner, Z. Liliental-Weber, J. Washburn, J. F. Klem, and J. Y. Tsao, Appl. Phys. Lett. **62**, 1536 (1993).
[27] See for example, E. A. Fitzgerald, S. B. Samavedam, Y. H. Xie, and L. M. Giovane, J. Vac. Sci. Technol. A **15**, 1048 (1997), and references therein.
[28] M. Gendry, V. Drouot, G. Hollinger, and S. Mahajan, Appl. Phys. Lett. **66**, 40 (1995).
[29] M. D. Pashley, K. W. Haberen, and J. M. Gaines, Appl. Phys. Lett. **58**, 406 (1991).
[30] P. Kightley, P. J. Goodhew, R. R. Bradley, and P. D. Augustus, J. Cryst. Growth **112**, 359 (1991).
[31] E. A. Stach, R. Hull, R. M. Tromp, M. C. Reuter, M. Copel, F. K. LeGoues, and J. C. Bean, J. Appl. Phys. **83**, 1931 (1998).
[32] K. W. Schwarz, Phys. Rev. Lett. **78**, 4785 (1997).
[33] G. P. Watson, Ph.D. thesis, Cornell University, 1992.
[34] G. P. Watson, M. O. Thompson, D. G. Ast, A. Fischer-Colbrie, and J. Miller, J. Electron. Mater. **19**, 957 (1990).
[35] M. J. Matragrano, D. G. Ast, J. R. Shealy, and V. Krishnamoorthy, J. Appl. Phys. **79**, 8371 (1996).
[36] R. S. Goldman, K. L. Kavanagh, H. H. Wieder, V. M. Robbins, S. N. Ehrlich, and R. M. Feenstra, J. Appl. Phys. **80**, 6849 (1996).
[37] R. S. Goldman, J. C. P. Chang, and K. L. Kavanagh, Proc. SPIE **2140**, 179 (1994), and references therein.
[38] N. D. Zakharov, Z. Liliental-Weber, W. Swider, A. S. Brown, and R. Metzger, Appl. Phys. Lett. **63**, 2809 (1993).
[39] M. R. Melloch, D. D. Nolte, J. M. Woodall, J. C. P. Chang, D. B. Janes, and E. S. Harmon, Crit. Rev. Solid State Mater. Sci. **21**, 189 (1996).
[40] K. H. Chang, R. Gibala, D. J. Srolovitz, P. K. Bhattacharya, and J. F.Mansfield, J. Appl. Phys. **67**, 4093 (1990).
[41] R. Beanland, M. Aindow, T. B. Joyce, P. Kidd, M. Lourenco, and P. J. Goodhew, J. Cryst. Growth **149**, 1 (1995).
[42] G. R. Fowles, in *Analytical Mechanics* (Saunders, Philadelphia, 1986), p. 17.